J Appl Electrochem (2015) 45:313–323
DOI 10.1007/s10800-015-0798-z

RESEARCH ARTICLE

Electrochemical characterizations of $LaMO_3$ (M = Co, Mn, Fe, and Ni) and partially substituted $LaNi_xM_{1-x}O_3$ (x = 0.25 or 0.5) for oxygen reduction and evolution in alkaline solution

K. Lopez · G. Park · H.-J. Sun · J.-C. An · S. Eom · J. Shim

Received: 27 October 2014 / Accepted: 2 February 2015 / Published online: 12 February 2015

Abstract Four transition metals, namely cobalt, iron, manganese, and nickel, were separately combined with lanthanum metal to synthesize $LaMO_3$ (M = Co, Fe, Mn, and Ni) perovskites using a sol–gel method. Electrodes for zinc–air rechargeable batteries were prepared with these perovskites and evaluated in terms of their morphology, crystal structure, electric conductivity, surface area, and particle size distribution. The electrochemical properties of the perovskites were characterized as catalysts of bifunctional electrodes for oxygen reduction reaction and oxygen evolution reaction in alkaline solution. Additionally, partially substituted $LaNi_x(M1, M2, or M3)_{1-x}O_3$ (x = 0.25 or 0.5, and M1, 2, 3 = Co, Fe, Mn) perovskites were synthesized to evaluate the effect of partial substitution of a metal in the Ni site, and improved physical and electrochemical properties were obtained.

K. Lopez · J. Shim (✉)
Department of Nano & Chemical Engineering, Kunsan National University, Kunsan, Jeonbuk 573-701, Korea
e-mail: jpshim@kunsan.ac.kr

G. Park
Department of Chemistry, Kunsan National University, Kunsan, Jeonbuk 573-701, Korea

H.-J. Sun
Department of Material Science & Engineering, Kunsan National University, Kunsan, Jeonbuk 573-701, Korea

J.-C. An
Research Institute of Industrial Science & Technology, Pohang, Gyeongbuk 790-330, Korea

S. Eom
Battery Research Center, Korea Electrotechnology Research Institute, Changwon 641-120, Korea

Keywords La-based perovskite · Bifunctional catalyst · Substituted $LaNi_xM_{1-x}O_3$ · Oxygen reduction · Oxygen evolution · Zn–air battery

1 Introduction

High specific energy, abundant and low-cost materials as well as low-risk operation make Zn–air batteries (100 W kg^{-1}) an attractive alternative energy storage system for different applications such as in back-up power generators, automobiles, portable devices, and electric vehicles. Zn–air batteries are classified as either primary or secondary systems. Primary Zn–air batteries have already been used as power supplies in hearing aids and certain military devices. On the other hand, secondary or rechargeable Zn–air batteries are still at development stage with a number of challenges yet to be overcome. These are related to the low performance and insufficient stability of the bifunctional air-electrode because of the complexity of the oxygen reduction and evolution reactions (ORR and OER) in the cathode [1–5]. An additional and critical problem yet to be solved concerns the irreversible reaction and dissolution of the Zn anode.

ORR and OER govern the discharging and charging of Zn–air batteries and are typically rate-limiting due to their slow and high overpotential kinetics. To improve the performance of Zn–air batteries, a catalyst would be required both capable of decreasing the resistances in the two reactions and stable enough to withstand intense oxidation (in ORR) and reduction (in OER), such a material is called as a bifunctional catalyst [6–8].

At present, the most efficient bifunctional catalysts for rechargeable metal-air batteries are precious metals [9]. However, their high cost, scarcity, and poor durability as

well as the limited performance of these electrocatalysts for ORR and OER limit their application for commercial use [10, 11].

Precious metal-free perovskite oxides are good alternative candidates because they provide bifunctional activity for both OER and ORR [12]. The composition of perovskite-structured metal oxides is generally ABO_3, where A is a rare earth element such as lanthanum metal and B is a transition metal. The non-stoichiometry of the cation or anion, the possible cation configuration distortion, and the mixed-valence electronic structure make perovskite materials to have flexible physical and chemical properties, enabling partial substitution of either the A- or B-site elements to optimize the desired property. Moreover, the low cost, abundance, and stability in alkaline solutions mean that perovskites are particularly attractive catalysts for Zn–air batteries. Indeed, a number of perovskites, viz. $LaCoO_3$, $LaMnO_3$, and $LaNiO_3$, have been studied for ORR catalysis, but their performance as the bifunctional catalysts for Zn–air batteries is not yet well established [12–16].

In this work, $LaMO_3$ (M = Co, Fe, Mn and Ni) and mixed $LaNi_x(M1,M2,M3)_{1-x}O_3$ ($x = 0.25$ or 0.5) perovskites were prepared using the Pechini-combustion method, and their bifunctional catalytic activity for Zn–air batteries was evaluated. The effects of different calcination temperatures were also determined, as was the influence of each transition metal on the physical and electrochemical properties of the synthesized perovskites.

2 Experimental

Perovskite powders were synthesized using the sol–gel method proposed by Pechini [17]. The $LaCoO_3$ (LCO) and $LaMnO_3$ (LMO) precursors were prepared by dissolving citric acid in deionized water at 60 °C under continuous stirring. Then, lanthanum nitrate ($La(NO_3)_3{\cdot}6H_2O$) was added followed by cobalt nitrate ($Co(NO_3)_2{\cdot}6H_2O$) or manganese nitrate ($Mn(NO_3)_2{\cdot}5H_2O$). After adding the metal nitrates, the temperature was increased to 90 °C at which point ethylene glycol was added. The mixture was stirred continuously for 2 h and the temperature was increased to 150 °C. The mixture was heated for 4–5 h until black powder was obtained. The resulting powder, the perovskite precursor, was pulverized and then calcined at 700 or 900 °C for 5 h. After calcination, the $LaMO_3$ perovskites were pulverized once more [18–20].

$LaFeO_3$ (LFO) and $LaNiO_3$ (LNO) precursors were similarly prepared but after heating at 150 voC for 4–5 h the powder samples were ignited and heated for another 5 h at 150 °C. Combustion is required to completely burn the organic constituents that are not charred by a simple heating [21, 22].

The effects of each of the four transition elements on the physical and electrochemical properties of the perovskites were evaluated by combining two or more transition metals in $LaMO_3$ perovskite to form four different $LaNi_x(M1, M2, \text{or } M3)_{1-x}O_3$ ($x = 0.25$ or 0.5) perovskites, namely $LaNi_{0.5}Mn_{0.5}O_3$ (LNM), $LaNi_{0.5}Fe_{0.5}O_3$ (LNF), $LaNi_{0.5}Mn_{0.25}Fe_{0.25}O_3$ (LNMF), and $LaNi_{0.25}Mn_{0.25}Fe_{0.25}Co_{0.25}O_3$ (LNMFC). The procedure for the preparation of these perovskites was identical to that for the LFO and LNO samples and the calcination temperature was fixed at 700 °C.

The morphology of the prepared perovskites was characterized by field-emission scanning electron microscopy (FE-SEM, Hitachi S-4800), their crystalline structure by X-ray diffraction (XRD, PANalytical), their electric conductivity by resistivity measurements (Changmin Tech, CMT-SR-100N), their surface area using Brunauer–Emmett–Teller (BET) analysis, and the particle size distribution by particle size analysis (PSA, HELOS/RODOX & SUCELL with Sympatec GmbH). For the electric conductivity measurements, the powder was pelletized with 20 % polymer binder (polyvinylidene fluoride, Arkema) and the resistance was measured using the four-point probe method.

For electrochemical characterization, an electrode was prepared by mixing the perovskites (70 wt%) with carbon black (30 wt%, Vulcan XC 72R) in a mortar and pestle with small volume of ethanol. The mixture was then transferred into a container followed by adding solvent (an equal amount of ethylene glycol and glycerol) and a few drops of Triton X-100 surfactant. Thereafter, the mixture was mechanically stirred for 2 h, PTFE was added as a binder, and mixing was prolonged for another 3 min. The resulting mixture was cast on an aluminum foil using a doctor blade with a thickness of 400 μm and then dried in an oven at 60 °C for 18 h and 120 °C for 4 h. The resulting sheet was transferred onto a wet-proofed carbon paper (Ballard Avcarb P50) by pressing at 10 MPa for 10 min at 280 °C. The electrode was baked in a furnace for 30 min at 350 °C. After cooling to room temperature, the electrode was weighed and cut into 2 cm in diameter. The electrode was then inserted into a cell frame containing 8 M KOH solution. The active area and catalyst loading amount of electrode were 1 cm^2 and 3.0 ± 0.5 mg cm^{-2}, respectively. The reference and counter electrodes were Zn wire (0.385 V vs. RHE) and Pt mesh, respectively. The electrochemical property of the perovskite was then measured using potentiostat/galvanostat (WBCS 3000, WonATech) over five cycles with voltage ranging from 0.8 to 2.5 V (vs. Zn) at a scan rate of 1 mV s^{-1} [23].

3 Results and discussion

The physical and electrochemical properties of $LaMO_3$ perovskites depend on the particular transition metal occupying the B site. The effects of transition metals with different sizes and shapes were evaluated by SEM. The SEM images of the synthesized perovskites calcined at 700 and 900 °C are shown in Figs. 1 and 2, respectively. The sample names indicated chemical composition followed by calcination temperature (e.g., LCO-700). In Fig. 1a–c, the particles in the LCO-, LFO-, and LMO-700 samples are smaller than in those with the same compositions calcined at 900 °C. Among the perovskite precursors calcined at 700 °C, LMO-700 has the smallest particles followed by LFO-700, then by LCO-700 and LNO-700. Among the perovskite precursors calcined at 900 °C, LFO-900 has the smallest particle size followed by LCO-900 and LMO-900, and then LNO-900. The particles less than 1 μm in diameter in LCO-900, LFO-900, and LMO-900 (Fig. 2a–c) agglomerate forming a porous microstructure. In LNO-900, the particles, shown in Fig. 2d, are mixed with small amounts of spherical and flake-like particles while the particles in LNO-700 (Fig. 1d) are irregular and smaller.

The use of the Pechini method and combined Pechini-combustion method ensures that crystalline perovskites are produced, as confirmed by the XRD patterns shown in Fig. 3a and b, obtained from the metal oxides calcined at 700 and 900 °C, respectively. LCO (ICSD 98-015-6452) perovskite has a hexagonal crystal structure in the *R-3c* space group [19, 21]; LFO (ICSD 98-015-3536) is orthorhombic with a *Pnma* space group; LMO (ICOD 01-086-1231) is rhombohedral with a *R-3c* space group; and LNO has orthorhombic symmetry in the *Fmmm* space group. The XRD patterns of perovskites formed at 700 °C (Fig. 3a) contain untraceable amounts of La_2O_3 and NiO. Those of LCO-900 and LMO-900 have small peaks that correspond to La_2O_3 (ICSD 98-002-8555, ICOD 00-005-0602, and ICOD 01-074-2430), while for LFO-900 and LNO-900, no trace of La_2O_3 is observed. The XRD pattern for LNO-900 has peaks that correspond to NiO (ICOD 01-089-7101).

The electric conductivities of the perovskites calcined at 700 and 900 °C are presented in Table 1. LNO is the most conductive perovskite followed by LMO and LCO, and then LFO. The $LaMO_3$ perovskites calcined at 700 °C are more conducting than those calcined at 900 °C because the particles are smaller and more tightly packed in the former than in the latter. The surface areas determined by BET analysis and the average particle sizes determined by PSA are shown in Table 1. The larger particles tend to have smaller surface areas. The particles (surface areas) in the perovskites calcined at 900 °C are larger (smaller) than in the perovskites calcined at 700 °C. Figure 4a and b shows the particle size distributions of $LaMO_3$ perovskites

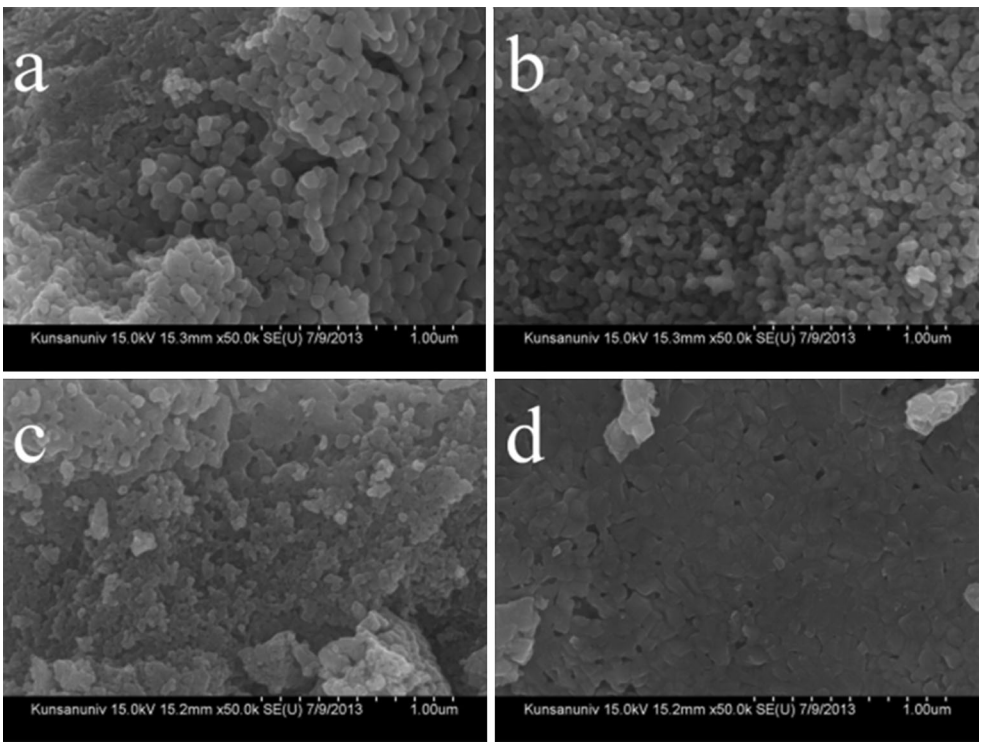

Fig. 1 SEM images of $LaMO_3$ (M = Co, Fe, Mn, and Ni) calcined at 700 °C. **a** $LaCoO_3$, **b** $LaFeO_3$, **c** $LaMnO_3$, and **d** $LaNiO_3$

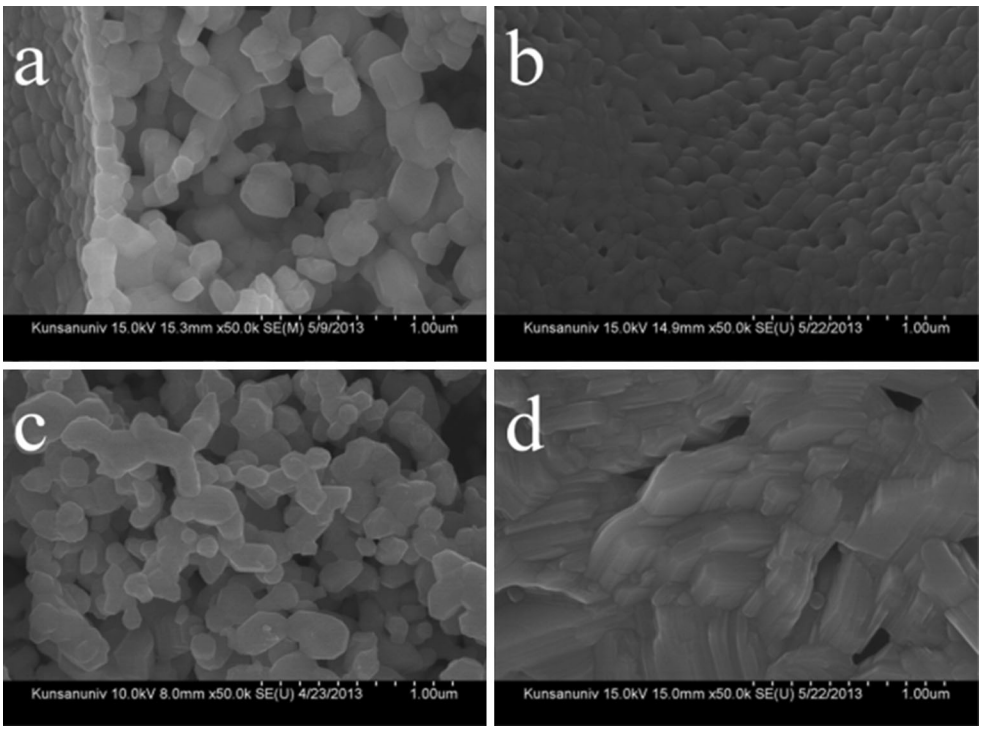

Fig. 2 SEM images of $LaMO_3$ (M = Co, Fe, Mn, and Ni) calcined at 900 °C. **a** $LaCoO_3$, **b** $LaFeO_3$, **c** $LaMnO_3$, and **d** $LaNiO_3$

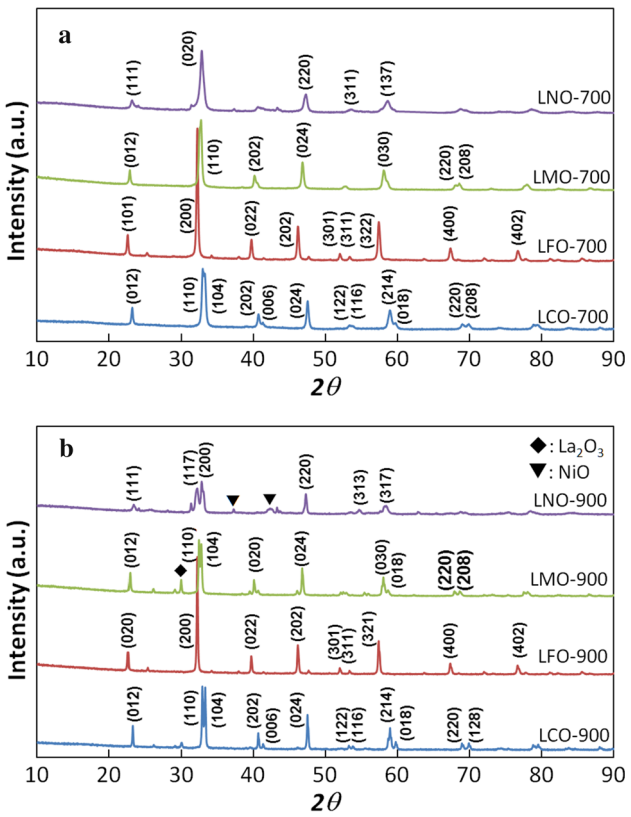

Fig. 3 XRD diffractions of $LaMO_3$ (M = Co, Fe, Mn, and Ni) perovskites calcined at 700 (**a**) and 900 °C (**b**)

calcined at 700 and 900 °C, respectively. The size distributions of $LaMO_3$ particles calcined at 900 °C are slightly shifted to larger sizes compared with those corresponding to the samples calcined at 700 °C.

The ORR and OER performances of the $LaMO_3$ (M = Co, Fe, Mn, and Ni) perovskites calcined at 700 and 900 °C are shown in Fig. 5a and b, respectively. After calcination at 700 °C, similar ORR performances are obtained for all samples, while LCO- and LNO-700 have the highest OER current density. LCO-900 shows the highest current density in OER among the perovskites calcined at 900 °C. For ORR, however, LMO-900 shows the highest performance, while the performances of LCO- and LNO-900 are similar. LFO-900 performs worst for both reactions.

Table 2 shows the current densities (I based on the apparent electrode area), mass activities (I_{MA} based on the mass of catalyst per 1 cm^2 of electrode), and specific activities (I_{SA} based on the surface area of the catalysts) at 1.0 and 2.4 V (vs. Zn) for ORR and OER. A similar ORR current density is measured for all perovskites calcined at 700 °C, while LCO-700 shows the highest current density for the OER. On the other hand, among the perovskites calcined at 900 °C, LMO-900 provides the highest current density for the ORR, followed by LCO-900, LNO-900, and LFO-900. For the OER, as for the samples calcined at 900 °C, the highest current density is measured for the

Table 1 Surface area, average particle size, and electric conductivity of $LaMO_3$ (M = Co, Fe, Mn, Ni) perovskites calcined at 700 and 900 °C

	Surface area ($m^2\ g^{-1}$)	Ave. particle size (μm)	Electric conductivity ($S\ cm^{-1}$)
LCO-700	13.06	9.52	8.3×10^{-6}
LFO-700	10.79	4.25	6.8×10^{-6}
LMO-700	14.16	10.04	2.2×10^{-5}
LNO-700	3.53	14.60	7.6×10^{-2}
LCO-900	3.79	19.05	4.8×10^{-8}
LFO-900	3.98	8.36	2.1×10^{-10}
LMO-900	6.23	5.93	1.6×10^{-6}
LNO-900	0.47	21.98	5.4×10^{-2}

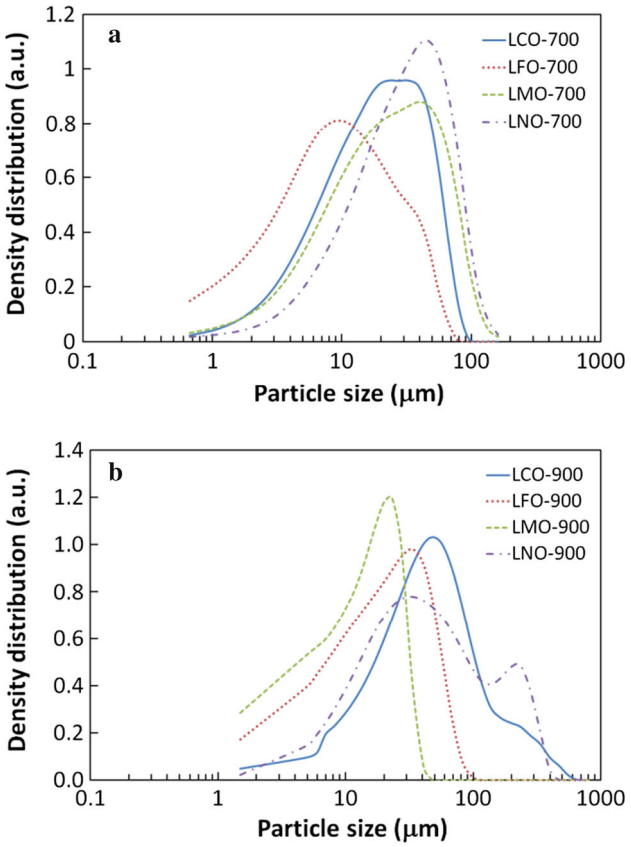

Fig. 4 Particle size distribution of $LaMO_3$ (M = Co, Fe, Mn, and Ni) perovskites calcined at 700 (**a**) and 900 °C (**b**)

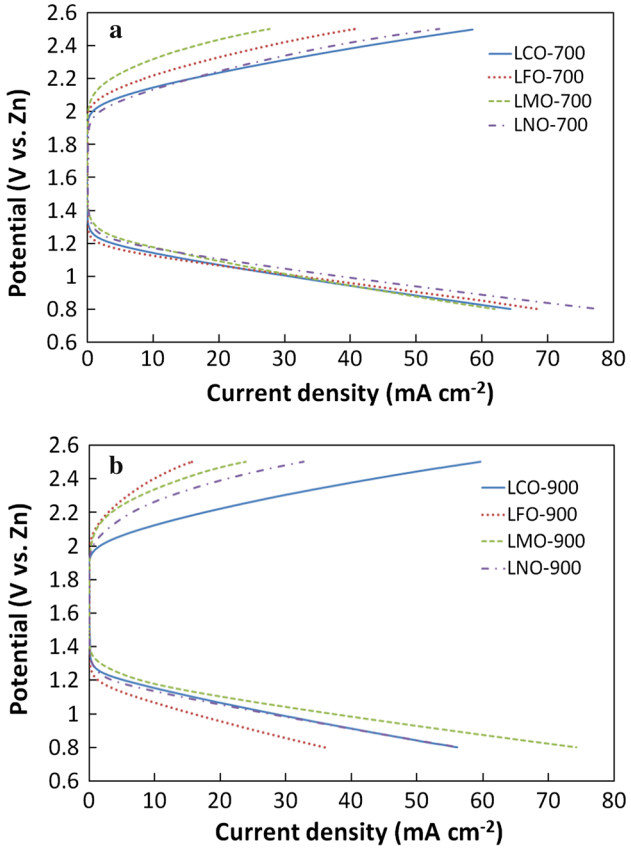

Fig. 5 Linear sweep voltammetries of $LaMO_3$ (M = Co, Fe, Mn, and Ni) perovskites calcined at 700 (**a**) and 900 °C (**b**) for ORR and OER

LCO-900 sample, but LMO-900 shows a lower current density than LNO-900. The mass activity is higher in the LCO and LMO samples calcined at 900 °C rather than 700 °C, but the opposite trend is observed for the other two samples. The specific activity of the catalysts increases with calcination temperature, such that the catalytic activity of the surface of the powder is greater following calcination at higher temperatures. Generally also, increasing the calcination temperature leads to greater crystallinity, and thereby to increased catalytic activity. However, this may cause the decrease of the surface areas induced by larger particles.

Figure 6a and b, respectively, shows the mass activity (based on the mass of catalyst in the electrode) and the specific activity (based on the surface area of the catalyst) as a function of the surface area of the catalyst. Although the points in Fig. 6a are somewhat scattered, there seems to be a slight increase in the mass activities for both ORR and OER with increasing the surface areas of the perovskite. This behavior therefore results from an increase in the contact area, the three-phase boundary, between the catalysts (solid), gas, and electrolyte (liquid) [24, 25]. Zhuang also noted that catalysts with high specific areas have enhanced electrocatalytic activity due to an increased number

Table 2 Current densities (I), mass activities (I_{MA}), specific activities (I_{SA}), and Tafel slopes (b) of $LaMO_3$ (M = Co, Fe, Mn, and Ni) perovskites calcined at 700 and 900 °C for ORR at 1 V and OER at 2.4 V (vs. Zn)

	ORR				OER			
	I^a (mA cm^{-2})	I^a_{MA} (mA mg^{-1})	I^a_{SA} (mA cm^{-2})	b (mV dec^{-1})	I^a (mA cm^{-2})	I^a_{MA} (mA mg^{-1})	I^a_{SA} (mA cm^{-2})	b (mV dec^{-1})
LCO-700	35.0	10.06	0.077	84.3	42.8	12.30	0.094	73.5
LFO-700	38.0	11.58	0.115	63.1	27.6	8.41	0.078	68.2
LMO-700	33.5	12.05	0.085	102.7	16.7	6.00	0.042	129.0
LNO-700	42.0	9.57	0.271	138.2	37.5	8.54	0.242	108.5
LCO-900	30.5	12.25	0.324	111.9	43.3	17.39	0.458	63.8
LFO-900	18.5	7.03	0.177	79.7	10.0	3.80	0.095	110.8
LMO-900	40.0	13.70	0.220	78.5	14.3	4.90	0.079	185.2
LNO-900	30.0	7.79	1.657	118.8	21.4	5.56	1.183	102.9

[a] At 1 V (vs. Zn) for ORR and 2.4 V (vs. Zn) for OER

of reaction sites [14]. The relationship between the ORR mass activity and the surface area is clearer than for the OER with a greater scatter. In Fig. 6b, a sharp decrease in surface activity is observed with increasing surface areas.

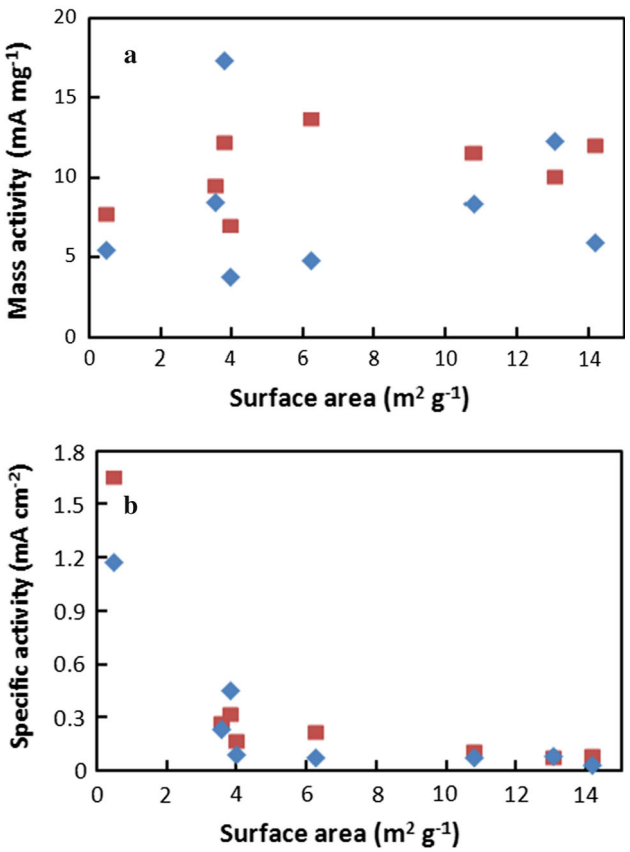

Fig. 6 Variation of mass activity **a** based on the weight of catalyst and specific activity **b** based on the surface area of catalyst of $LaMO_3$ (M = Co, Fe, Mn, and Ni) perovskites for ORR (*closed square*) and OER (*closed diamond*) as a function of surface area of catalyst

This means that larger surface areas do indeed increase the number of reaction sites and thereby the catalytic activity, but the activity per reaction site is lower. The effect of the electric conductivity of the catalyst was also investigated (data not shown), but this showed no correlation with the catalytic activity. As reported by Zhuang, the activity of the catalyst correlates to its surface area much more than to its conductivity.

Figure 7 shows Tafel plots for the $LaMO_3$ perovskites, in which the data from Fig. 5 are plotted as potential versus current density on a logarithmic scale. Table 2 shows the Tafel slopes obtained for the ORR and OER, respectively. For the perovskites calcined at 700 °C, LCO-700 and LFO-700 have lower Tafel slopes than LMO-700 and LNO-700. The Tafel slopes are steeper for the samples calcined at the higher temperature, 900 °C, the only exception being LNO-900 for which the Tafel slope decreases. Singh et al. reported OER Tafel slopes for sol–gel synthesized $LaMnO_3$, $LaNiO_3$, and $LaCoO_3$ of ~110 [26], 65 [27], and ~65 mV dec^{-1} [28], respectively. Kiros and co-workers measured an ORR Tafel slope for $LaNiO_3$ of 125 mV dec^{-1} [29]. Suresh et al. reported Tafel slopes in $La_{0.9}Sr_{0.1}FeO_3$ synthesized by solution combustion of 105–120 mV dec^{-1} and 62–67 mV dec^{-1} for ORR and OER, respectively [30]. The Tafel slopes reported here for $LaCoO_3$, $LaMnO_3$, and $LaNiO_3$ are therefore similar to those in the literature, $LaFeO_3$ excepted. The relationships between the Tafel slopes and the surface areas or the conductivities of the materials are shown in Fig. 8. It is well known that the Tafel slope is strongly related to the nature of the materials. Here, no correlation is observed between the Tafel slopes and the surface areas or electric conductivities. This means that the Tafel slope is not affected by the physical properties of the materials.

As listed in Table 2, LCO-900 showed the highest catalytic activity for the OER, while LNO-700, LMO-900,

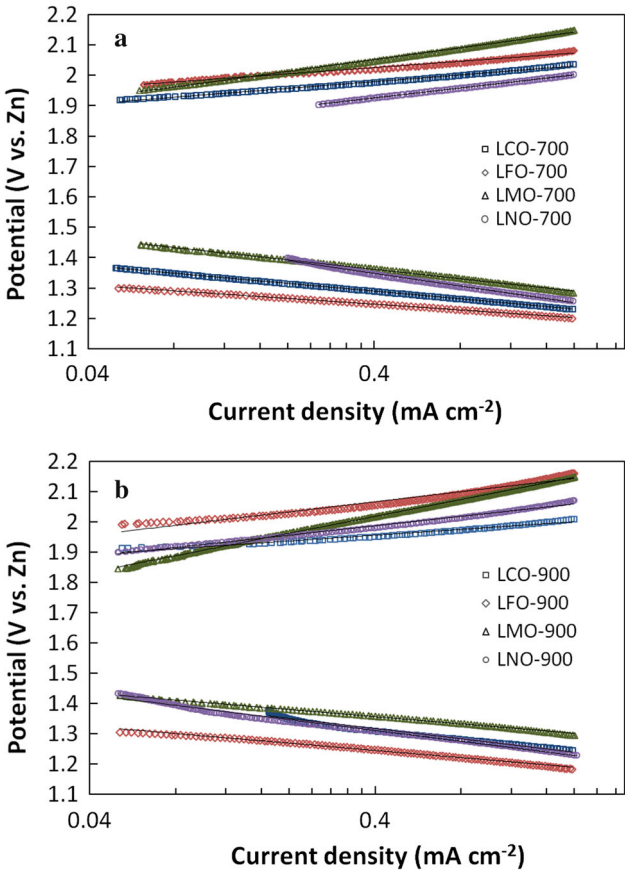

Fig. 7 Tafel plots of $LaMO_3$ (M = Co, Fe, Mn, and Ni) perovskites calcined at 700 (**a**) and 900 °C (**b**) for ORR and OER

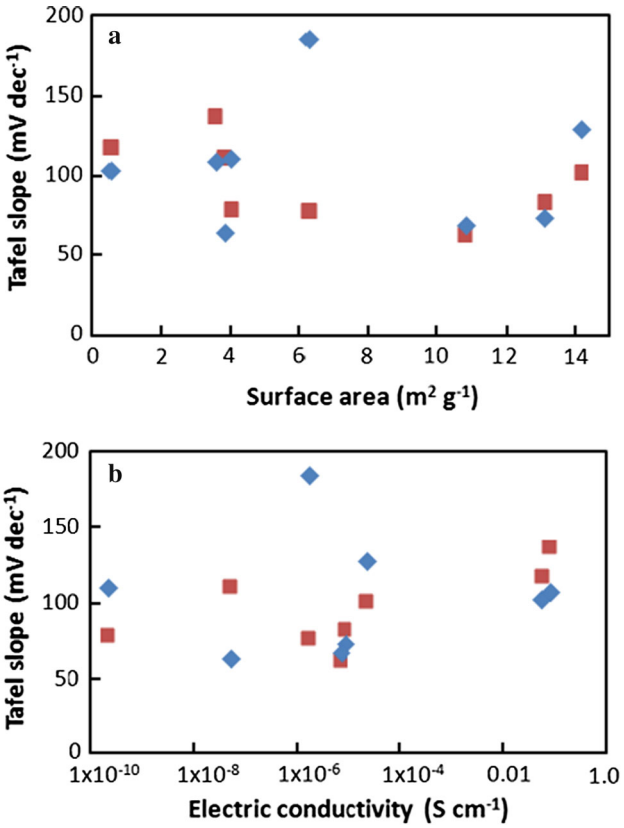

Fig. 8 Variation of Tafel slope as a function of the surface area (**a**) and the electric conductivity (**b**) of the catalyst of $LaMO_3$ (M = Co, Fe, Mn, or Ni) perovskites calcined at 700 and 900 °C for ORR (*closed square*) and OER (*closed diamond*)

LCO-900, and LNO-900 showed better performance than others. The electrochemical performances of the perovskites calcined at 900 °C were relatively better than those of the perovskites calcined at 700 °C. It means that the activity of the perovskite calcined at high temperature is improved in spite of decreasing the surface area. Thus, LCO-900 may be appropriate material for the ORR and OER as the catalyst of bifunctional electrode.

Previous studies have noted that the metal ion occupying the B site in the perovskites is the main factor governing the oxidative catalytic reaction because of its ability to shift from one oxidation state to another [20]. Even if $LaCoO_3$ showed relatively better performance than others, $LaNiO_3$ was selected because of its relatively high current density, its intrinsic ORR activity comparable to that of Pt/C, its metal-like electric conductivity and inadequate results for ORR and OER in literatures [12, 16, 31]. Ni in $LaNiO_3$ was therefore partially substituted by Mn and/or Fe and/or Co to improve the properties of the perovskites and to investigate the influence thereon of different metals. Samples with the composition $LaNi_xM_{1-x}O_3$ were obtained thereby, with $x = 0.25$ or 0.5.

The SEM images of the LNM-700, LNF-700, LNMF-700, and LNMFC-700 are shown in Fig. 9. The micrographs show less particle agglomeration than for the unsubstituted $LaMO_3$ perovskites. Partial substitution in the Ni site should indeed provide smaller particles. Similar XRD patterns and peak positions are obtained for the four partially substituted $LaNi_xM_{1-x}O_3$ powders, as shown in Fig. 10. The peaks in the XRD pattern correspond to those observed for the $LaMO_3$ perovskites in Fig. 3. The surface area, average particle size, and electric conductivity of the $LaNi_xM_{1-x}O_3$ perovskites are also listed in Table 3. In comparison with the values shown in Table 1, the partial substitution of $LaNi_xM_{1-x}O_3$ leads to much smaller particles and larger surface areas. In terms of conductivity, Table 3 shows that LNF-700 is the most conductive perovskite followed by LNMF-700, LNM-700, and lastly by LNMFC-700. Comparing these values with those in Table 1 shows that the partial substitution of the Ni ion increases the conductivity of the LMO and LFO perovskites. It is well known that the surface area and the particle size in perovskites are inversely proportional. The particle size distributions obtained for the $LaNi_xM_{1-x}O_3$

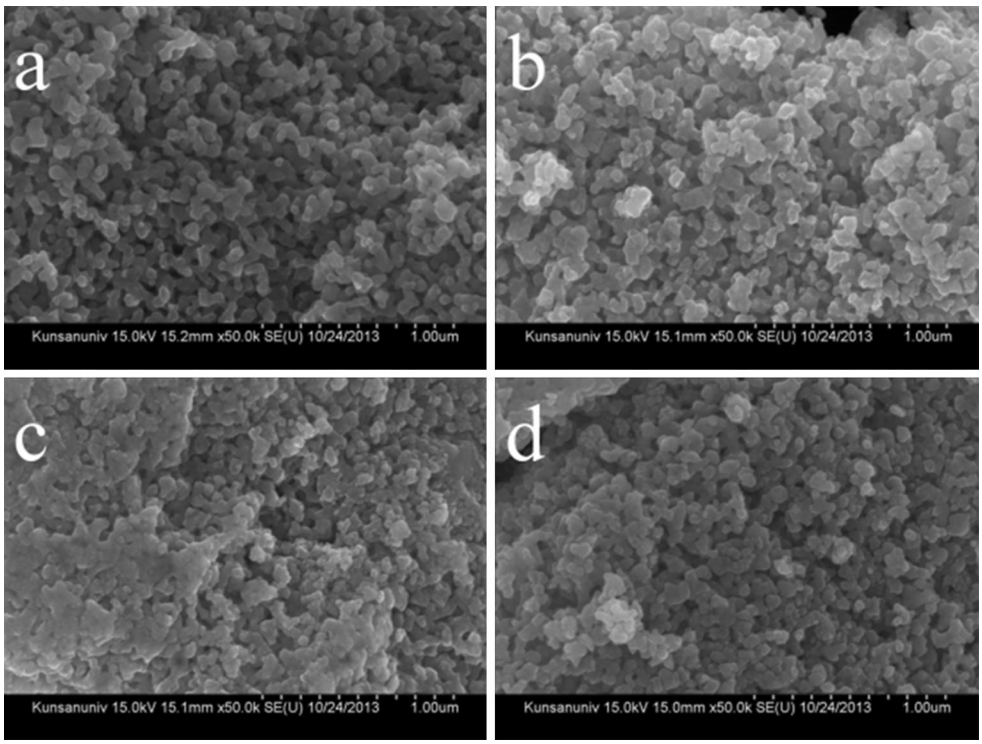

Fig. 9 SEM images of LNM-700 (**a**), LNF-700 (**b**), LNMF-700 (**c**), and LNMFC-700 (**d**)

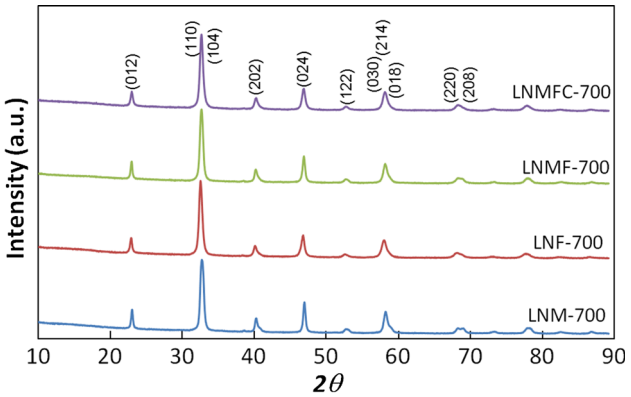

Fig. 10 XRD pattern of $LaNi_x(M1, M2, or M3)_{1-x}O_3$ ($x = 0.25$ or 0.5, and M1, 2, 3 = Co, Fe, or Mn) perovskites calcined at 700 °C

perovskites are shown in Fig. 11. The partially substituted perovskite particles are between 0.5 and 120 μm in diameter. The particle size distributions are similar in the unsubstituted perovskites calcined at the same temperature, but in the partially substituted perovskites, the particles are slightly smaller.

The linear sweep voltammograms and Tafel plots of $LaNi_xM_{1-x}O_3$ perovskites for the ORR and OER are shown in Fig. 12 and Table 4. The order of the samples in terms of current density in the OER is LNMF > LNF > LNMFC ≅ LNM. Similarly, in terms of ORR performance, the order is LNF ≅ LNM > LNMF > LNMFC. In particular, the LNF sample shows a higher catalytic activity than either the LNO

Table 3 Surface area, average particle size, and electric conductivity of $LaNi_x(M1,M2,M3)_{1-x}O_3$ (M1,2,3 = Co, Fe, and Mn) perovskites calcined at 700 °C

	Surface area ($m^2\ g^{-1}$)	Ave. particle size (μm)	Electric conductivity ($S\ cm^{-1}$)
LNM-700	8.79	6.45	3.8×10^{-6}
LNF-700	7.10	6.37	1.7×10^{-2}
LNMF-700	8.84	3.92	7.8×10^{-6}
LNMFC-700	9.28	5.03	2.7×10^{-6}

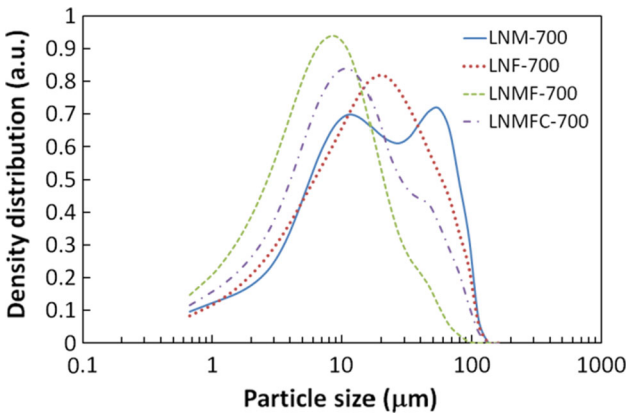

Fig. 11 Particle size distribution of $LaNi_x(M1, M2, or M3)_{1-x}O_3$ ($x = 0.25$ or 0.5, and M1, 2, 3 = Co, Fe, or Mn) perovskites calcined at 700 °C

or LFO. Hyodo et al. reported that unsubstituted perovskites, such as $LaMnO_3$ and $LaCoO_3$, showed better performance than partially substituted ones, but for $LaNiO_3$ and $LaFeO_3$ the partial substitutions of B site lead to increased activity [32]. Partially substituted perovskites generally show higher catalytic performance than non-substituted perovskites, even though their surface areas are similar. The Tafel slopes listed in Table 4 are much shallower for the partially substituted $LaNi_xM_{1-x}O_3$ perovskites than unsubstituted $LaNiO_3$, except for the LNM-700 sample in the OER.

The Tafel slopes are plotted in Fig. 13 as a function of the Fe or Mn content in the Ni-based perovskites. Figure 13a shows that the partial substitution of Fe in $LaNiO_3$ leads to shallower Tafel slopes in the ORR and OER than for unsubstituted $LaNiO_3$ and $LaFeO_3$, while the addition

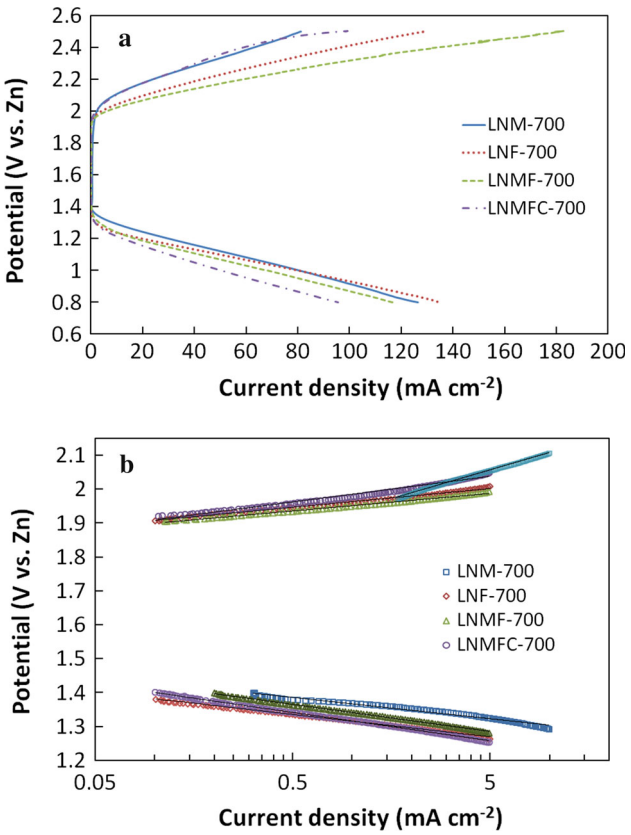

Fig. 12 Linear sweep voltammetry and Tafel plots for ORR and OER of $LaNi_x(M1, M2, or M3)_{1-x}O_3$ ($x = 0.25$ or 0.5, and M1, 2, 3 = Co, Fe, or Mn) perovskites calcined at 700 °C for ORR and OER

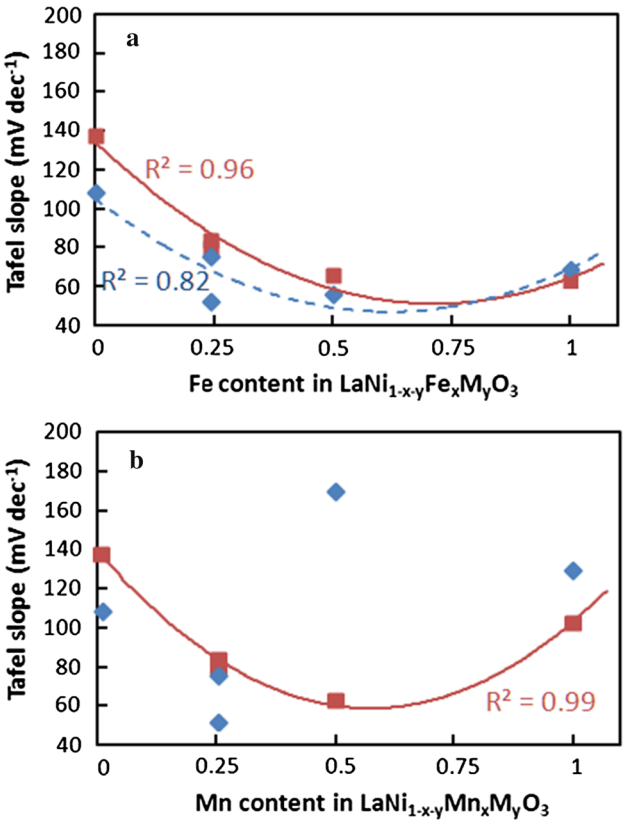

Fig. 13 Variation of Tafel slopes as a function of Fe (**a**) and Mn (**b**) content in $LaNi_xM_{1-x}O_3$ perovskites calcined at 700 °C for ORR (*closed square*, *continuous line*) and OER (*closed diamond*, *dotted line*). $LaNi_x(M1, M2, or M3)_{1-x}O_3$ ($x = 0$, 0.25, 0.5, or 1, and M1, 2, 3 = Co, Fe, or Mn) perovskites (LNO, LFO, LMO, LNM, LNF, LNMF, and LNMFC)

Table 4 Current densities (I), mass activities (I_{MA}), specific activities (I_{SA}), and Tafel slopes (b) of $LaNi_x(M1,M2,M3)_{1-x}O_3$ (M1,2,3 = Co, Fe, Mn) perovskites calcined at 700 °C for ORR at 1 V and OER at 2.4 V (vs. Zn)

	ORR				OER			
	I^a (mA cm^{-2})	I^a_{MA} (mA mg^{-1})	I^a_{SA} (mA cm^{-2})	b (mV dec^{-1})	I^a (mA cm^{-2})	I^a_{MA} (mA mg^{-1})	I^a_{SA} (mA cm^{-2})	b (mV dec^{-1})
LNM-700	79.0	25.8	0.294	62.9	59.1	19.3	0.220	170.0
LNF-700	83.0	35.3	0.496	66.1	96.8	41.2	0.580	55.5
LNMF-700	69.0	23.2	0.262	79.9	133.2	44.8	0.507	51.8
LNMFC-700	52.0	22.9	0.247	83.8	58.7	25.9	0.279	75.5

[a] At 1 V (vs. Zn) for ORR and 2.4 V (vs. Zn) for OER

of Mn decreases the Tafel slope only for the ORR, as shown in Fig. 13b. 25 % Mn in the Ni-based perovskites shows low Tafel slope in the OER because the sample contains 25 % Fe. As shown in Figs. 12 and 13, other than for the effect of Mn addition on the OER, the partial substitution of the metal in the B site of ABO_3 perovskites leads to improved catalytic activity in both the ORR and OER.

For various La-based perovskites, the variation of their electrochemical parameters was investigated on physical properties, surface area and electric conductivity, and chemical composition. Conclusively, their catalytic activities were strongly related to the intrinsic nature of perovskite rather than their physical properties, even if the increase of the surface area could improve the cell performance.

4 Conclusions

$LaMO_3$ (M = Co, Fe, Mn, and Ni) perovskites were synthesized as bifunctional catalysts for Zn–air batteries, and their catalytic activities for the ORR and OER were evaluated in the alkaline solution. The physical and electrochemical properties of the perovskite materials varied with the calcination temperature, with 900 °C proving more effective in this regard than 700 °C. In cell tests for ORR and OER, $LaCoO_3$ performed best among the different perovskites, even though its electric conductivity was relatively low compared to that of the other samples. The catalytic activity of highly conductive $LaNiO_3$ can be improved by the partial substitution of the Ni ion with one or more of the transition elements, Mn, Fe, and/or Co. The partial substitution of Ni in $LaNiO_3$ led to more favorable physical and electrochemical properties; adding Fe led to improved catalytic activity both in the ORR and OER, while with Mn, only the ORR activity was improved.

Acknowledgments This work was supported by the National Research Foundation of Korea Grant funded by the Korean Government (MEST) (NRF-2012-M1A2A2-029538).

References

1. Hilder M, Winther-Jensen B, Clark NB (2012) The effect of binder and electrolyte on the performance of thin zinc–air battery. Electrochim Acta 69:308–314
2. Wang X, Sebastian PJ, Smit MA, Yang H, Gamboa SA (2003) Studies on the oxygen reduction catalyst for zinc–air battery electrode. J Power Sources 124:278–284
3. Li X, Qu W, Zhang J, Wang H (2010) Electrocatalytic activities of perovskite toward oxygen reduction reaction in concentrated alkaline electrolytes. ESC Trans 28:45–56
4. Lee SH, Jeong Y, Lim S, Lee EA, Yi CW, Kim K (2010) The stable rechargeability of secondary Zn–air batteries: is it possible to recharge a Zn–air battery? J Korean Electrochem Soc 13:45–49
5. Wang T, Kaempgen M, Nopphawan P, Wee G, Mhaisalkar S, Srinivasan M (2010) Silver nanoparticle-decorated carbon nanotubes as bifunctional gas-diffusion electrodes for zinc–air batteries. J Power Sources 195:4350–4355
6. Lee JS, Kim ST, Cao R, Choi NS, Liu M, Lee KT, Cho J (2011) Metal-air batteries with high energy density: Li–air versus Zn–air. Adv Energy Mater 1:34–50
7. Shim J, Park YS, Lee HK, Park SG, Lee JS (1996) Oxygen reduction reaction of $La_{1-x}Ca_xCoO_3$ of gas diffusion electrode in alkaline fuel cell. J Korean Ind Eng Chem 7:992–998
8. Jorissen L (2006) Bifunctional oxygen/air electrodes. J Power Sources 155:23–32
9. Chen Z, Choi JY, Wang H, Li H, Chen Z (2011) Highly durable and active non-precious air cathode catalyst for zinc air battery. J Power Sources 196:3673–3677
10. Chen Z, Yu A, Higgins D, Li H, Wang H, Chen Z (2012) Highly active and durable core-corona structured bifunctional catalyst for rechargeable metal-air battery application. Nano Lett 12:1946–1952
11. Zhou W, Sunarso J (2013) Enhancing Bi-functional electrocatalytic activity of perovskite by temperature shock: a case study of $LaNiO_{3-\delta}$. J Phys Chem Lett 4:2982–2988
12. Hardin WG, Slanac DA, Wang X, Dai S, Johnston KP, Stevenson KJ (2013) Highly active, nonprecious metal perovskite electrocatalysts for bifunctional metal-air battery electrodes. J Phys Chem Lett 4:1254–1259
13. Zhang H, Li N, Li K, Xue D (2007) Structural stability and formability of ABO_3-type perovskite compounds. Acta Crystallogr Sect B 63:812–818
14. Zhuang S, Liu S, Huang C, Tu F, Zhang J, Li Y (2012) Electrocatalytic activity of nanoporous perovskite $La_{1-x}Ca_xCoO_3$ towards hydrogen peroxide reduction in alkaline medium. Int J Electrochem Sci 7:338–344
15. Neburchilov V, Wang H, Martin JJ, Qu W (2010) A review on air cathodes for zinc–air fuel cells. J Power Sources 195:1271–1291
16. Suntivich J, Gasteiger HA, Yabuuchi N, Nakanishi H, Goodenough JB, Shao-Horn Y (2011) Design principles for oxygen-reduction activity on perovskite oxide catalysts for fuel cells and metal-air batteries. Nat Chem 3:546–550
17. Pechini MP (1967) Method of preparing lead and alkaline earth titanates and niobates and coating method using the same to form a capacitor. US Patent No. 3.330.697
18. Popa M, Kakihana M (2002) Synthesis of lanthanum cobaltite ($LaCoO_3$) by the polymerizable complex route. Solid State Ion 151:251–257
19. Kuo JH, Anderson HU, Sparlin DM (1990) Oxidation-reduction behavior of undoped and Sr-doped $LaMnO_3$: defect structure, electrical conductivity, and thermoelectric power. J Solid State Chem 87:55–63
20. Worayingyong A, Kangvansura P, Ausadasuk S, Praserthdam P (2008) The effect of preparation: Pechini and Schiff base methods, on adsorbed oxygen of $LaCoO_3$ perovskite oxidation catalysts. Colloids Surf A 315:217–225
21. Popa M, Frantti J, Kakihana M (2002) Characterization of LaMeO3 (Me: Mn Co, Fe) perovskite powders obtained by polymerizable complex method. Solid State Ion 154–155:135–141
22. Fernandes JDG, Melo DMA, Zinner LB, Salustiano CM, Silva ZR, Martinelli AE, Cerqueira M, Alves Júnior C, Longo E, Bernardi MIB (2002) Low-temperature synthesis of single-phase crystalline $LaNiO_3$ perovskite via Pechini method. Mater Lett 53:122–125
23. Ahn S, Kim K, Kim H, Nam S, Eom S (2010) Synthesis and electrochemical performance of $La_{0.7}Sr_{0.3}Co_{1-x}Fe_xO_3$ catalysts for zinc air secondary batteries. Phys Scr T139:014014

24. Matsushima H, Majima W, Fukunaka Y (2013) Three-phase interfacial phenomena in alkaline unitized regenerative fuel cell. Electrochim Acta 114:509–513
25. Matsuno Y, Suzawa K, Tsutsumi A, Yoshida K (1996) Characteristics of three-phase fluidized-bed electrodes for an alkaline fuel cell cathode. Int J Hydrog Energy 21:195–199
26. Singh NK, Lal B, Singh RN (2002) Electrocatalytic properties of perovskite-type $La_{1-x}Sr_xMnO_3$ obtained by a novel sol–gel route for O_2 evolution in KOH solutions. Int J Hydrogen Energy 27:885–893
27. Singh RN, Tiwari SK, Singh SP, Jain AN, Singh NK (1997) Electrocatalytic activity of high specific surface area perovskite-type $LaNiO_3$ via sol–gel route for electrolytic oxygen evolution in alkaline solution. Int J Hydrog Energy 22:557–562
28. Lal B, Raghunandan MK, Gupta M, Singh RN (2005) Electrocatalytic properties of perovskite-type $La_{1-x}Sr_xCoO_3$ ($0 \leq \times \leq 4$) obtained by a novel stearic acid sol–gel method for electrocatalysis of O_2 evolution in KOH solutions. Int J Hydrog Energy 30:723–729
29. Bursell M, Pirjamali M, Kiros Y (2002) $La_{0.6}Ca_{0.4}CoO_3$, $La_{0.1}Ca_{0.9}MnO_3$ and $LaNiO_3$ as bifunctional oxygen electrodes. Electrochim Acta 47:1651–1660
30. Suresh K, Panchapagesan TS, Patil KC (1999) Synthesis and properties of $La_{1-x}Sr_xFeO_3$. Solid State Ion 126:299–305
31. Sarma DD, Shanthi N, Barman SR (1995) Band Theory for Ground-State Properties and Excitation Spectra of Perovskite LaMO3 (M = Mn, Fe Co, Ni). Phys Rev Lett 75:1126–1129
32. Hyodo T, Shimizu Y, Miura N, Yamazoe N (1994) Investigation of materials for gas diffusion-type oxygen cathode aiming at electric power-saving brine electrolysis. Denki Kagaku 62:158–164